Article

Bimetallic ZIF-8 from Hydroxide Double Salts for Efficient Cu²⁺ Removal in Wastewater

Yixin Chen, Zexi Chen, and Sheng Chu*

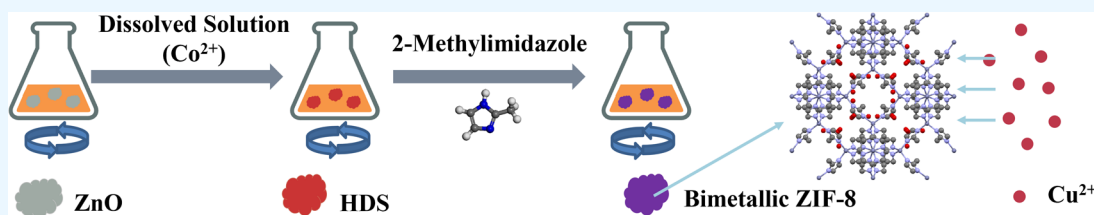Cite This: *ACS Omega* 2025, 10, 4326−4335

Read Online

ACCESS | Metrics & More | Article Recommendations | Supporting Information

ABSTRACT: Metal−organic frameworks (MOFs) hold significant potential for applications in gas adsorption and separation, catalysis, chemical sensing, and drug delivery. Zeolitic imidazolate frameworks (ZIFs) are a type of MOF composed of metal ions and imidazolate ligands, structurally similar to zeolite structures. ZIF-8, a widely studied ZIF material, is composed of zinc ions (Zn^{2+}) and 2-methylimidazole as fundamental building blocks featuring unique porous structures, a high specific surface area, and excellent thermal and chemical stability. This study introduces a rapid room-temperature synthesis method for bimetallic ZIF-8 through the hydroxide double salt (HDS) precursor. Various characterization techniques confirmed that the synthesized bimetallic ZIF-8 exhibits uniform particle size and high crystallinity. Experimental results indicate that the HDS precursor provides numerous active sites, facilitating rapid nucleation and resulting in uniformly sized bimetallic ZIF-8 particles. By optimizing the ultrasonic time of HDS, the concentration of 2-methylimidazole, and the reaction time, the synthesis conditions were refined, producing bimetallic ZIF-8 particles with an average size of 135.0 nm and a minimum polydispersity index (PDI) of 0.024. Additionally, the copper ion adsorption performance was evaluated, with the synthesized bimetallic ZIF-8 showing the highest adsorption capacity of 1196.82 mg/g at pH 6, demonstrating its effectiveness in heavy metal removal.

1. INTRODUCTION

Metal−organic frameworks (MOFs) have extensive application prospects in areas such as gas adsorption and separation, catalysis, chemical sensing, and drug delivery.[1] Zeolitic Imidazolate Frameworks (ZIFs), a type of MOF, are composed of metal ions and imidazolate ligands, resembling the structure of zeolites.[2] Among these, ZIF-8 is a common ZIF material, composed of zinc ions (Zn^{2+}) and 2-methylimidazole. It possesses unique porous structures, high specific surface areas, and excellent thermal and chemical stability,[3] making it highly suitable for diverse applications in heavy metal adsorption,[4−7] gas separation, catalysis, and energy storage.[8−12]

In recent years, bimetallic ZIF materials have garnered significant attention due to the synergistic effects between two metal ions that can enhance their performance in various applications.[13−15] For instance, introducing a second metal ion into ZIF-8 can adjust the material's adsorption properties, improve its chemical stability, and enhance its selectivity toward specific metal ions.[16,17] In the case of copper ion adsorption,[18−20] the combination of zinc ions with another transition metal, such as cobalt ions, can significantly increase the adsorption capacity and recyclability, making bimetallic ZIF-8 a promising candidate for wastewater treatment.[21,22] Furthermore, the design incorporating multiple metal centers offers opportunities to tailor the electronic and structural properties of the material, thereby expanding its potential applications.[23−25]

Nanomaterials with uniform particle sizes typically exhibit better dispersibility, higher specific surface areas, and more stable physicochemical properties.[26,27] The self-assembly of particles into three-dimensional ordered superstructures is crucial for designing materials such as plasmonic sensors, energy or gas storage systems, catalysts, and photonic crystals.[28] For ZIF-8, uniform particle size can facilitate the formation of regular self-assembled structures, enhancing its performance in gas adsorption, catalysis, and separation applications.[29,30] Studies combining experimental and simulation data have demonstrated that truncated rhombic dodecahedral ZIF-8 particles can self-assemble into millimeter-sized superstructures with underlying three-dimensional rhombic lattices, functioning as photonic crystals.[31] These

4326
https://doi.org/10.1021/acsomega.4c06512
ACS Omega 2025, 10, 4326−4335

Table 1. Advantages and Disadvantages of Various ZIF Synthesis Methods

methods	advantages	disadvantages
microwave-assisted synthesis method[35,36]	rapid reaction	high energy cost
	phase selectivity	thermally assisted
	small product size	specialized reaction apparatus
ultrasonic chemical synthesis method[37,38]	simple operation	difficult to control the reaction
	product selectivity	high energy cost
	short reaction time	expensive reaction apparatus
mechanochemical synthesis method[39]	solvent-free conditions	limited synthesis systems
	economical and environmentally	
electrochemical synthesis method[40]	mild reaction conditions	complex reaction apparatus
	simple operation	only applicable to redox reactions
	avoids anion formation	insufficient theory and process development
flow chemistry method[41]	scalable production	some inherent risks
	green and economical	some limitations
		requires precise control
layered compound transformation method	rapid reaction	still in the early research stage, requiring further investigation into more systems
	high space-time yield	
	versatility	

superstructures can adjust photonic band gaps by controlling the particle size of ZIF-8 and interacat with guest substances in the micropores of ZIF-8 particles. Uniformly distributed ZIF-8 nanoparticles are expected to form these ordered super-structures, potentially advancing the application of three-dimensional photonic materials.[32−34]

these methods. To better illustrate the strengths and limitations of various ZIF synthesis methods, Table 1 provides a comparative summary of their advantages and disadvantages. The HDS formula is summarized as $M_{1-x}^{2+}(M')_x^{2+}(OH)_{2-y}A_{y/n}^{n-}\cdot mH_2O$, where M and M′ are divalent metal cations like Co, Cu, Zn, Mn, Ni, Mg, Cd, and Fe. Anions (A⁻) such as CH_3COO^-, NO_3^-, Cl^-, SO_4^{2-}, and CO_3^{2-} balance the positively charged layers, which consist of metal hydroxides interconnected by inorganic/organic inter-layer anions.[42] HDS compounds exhibit excellent anion exchange properties due to the exchange of bound anions within the hydroxide layers.

The transformation of HDS into MOFs follows a typical pathway: (1) interlayer anions exchange with organic ligands; (2) the positively charged layers facilitate molecular transport; (3) high mobility of interlayer anions allows rapid coordination with metal cations. For example, the transformation of HDS into HKUST-1 can occur in under 1 min at room temperature, with a high space-time yield (STY) of $>3.6 \times 10^4$ kg·m⁻³·d⁻¹.[43] This demonstrates the potential of HDS-based MOF synthesis for green and efficient industrial production. Additionally, this method can be used to create MOF composites with specialized structures like MOF fibers, hierarchical porous MOFs (HP-MOFs), and MOF membranes.[44,45] The rapid transformation of CuZnHDS into HKUST-1 at room temper-ature remains the most common example, though further system development is needed.

This study proposes a rapid room-temperature synthesis method for ZIF-8 based on HDS precursors. The multiple reactive sites of HDS precursors lead to the formation of uniformly sized bimetallic ZIF-8 particles, creating ideal conditions for self-assembly. We conducted detailed morpho-logical, structural, and specific surface area characterizations to investigate the uniformity and potential self-assembly proper-ties of bimetallic ZIF-8 particles synthesized from HDS precursors. By adjusting the synthesis conditions, we controlled the particle size distribution of bimetallic ZIF-8, producing a series of uniformly sized bimetallic ZIF-8 nanoparticles. The results demonstrate that this novel synthesis method not only simplifies the ZIF-8 preparation process but also enhances particle size uniformity, underscoring its potential for practical applications.

2. EXPERIMENTAL SECTION

2.1. Materials. In this experiment, unless otherwise specified, all reagents used were commercially available analytical grade and used as received. The specific reagents and materials used are as follows: zinc oxide (ZnO, 99% purity) was purchased from Macklin; cobalt nitrate hexahy-drate ($Co(NO_3)_2\cdot 6H_2O$, 99.99% purity) was purchased from Aladdin; zinc nitrate hexahydrate ($Zn(NO_3)_2\cdot 6H_2O$, 99% purity) was purchased from Aladdin; 2-methylimidazole ($C_4H_6N_2$, 98% purity) was purchased from Macklin; ethanol (CH_3CH_2OH, 99.7% purity) was purchased from Macklin.

2.2. Sample Preparation. *2.2.1. Synthesis of CoZnHDS via the Hydrolysis Method.* First, 1.0 g (12.28 mmol) of ZnO powder was dispersed in 10 mL of deionized water using ultrasound treatment for 10 min. Next, 4.465 g (15.34 mmol) of $Co(NO_3)_2\cdot 6H_2O$ was dissolved in 15 mL of deionized water. Under vigorous stirring at room temperature, the $Co(NO_3)_2\cdot 6H_2O$ solution was slowly added to the ZnO suspension. The mixture (molar ratio Co/Zn = 1.25:1) was stirred magnetically at room temperature for 12 h. After vacuum filtration, the pink powder was collected and stirred at room temperature in 25 mL of 0.64 M $Co(NO_3)_2$ solution. After 12 h of continuous stirring, ZnO was completely converted to HDS. The HDS powder was collected by vacuum filtration and washed with 50 mL of ethanol for 6 h. The resulting slurry was then centrifuged at 6000 rpm for 5 min, and the resulting powder was dried overnight in a vacuum oven at 25 °C. The HDS synthesized via the hydrolysis method is designated as CoZnHDS.

2.2.2. Conversion of CoZnHDS to Bimetallic ZIF-8. First, 0.05 g of CoZnHDS was dispersed in 10 mL of a mixed solvent of deionized water and ethanol (v%/v% = 50:50) using ultrasound treatment for 10 min. Then, 0.5 g (6.1 mmol) of 2-methylimidazole was dissolved in 5 mL of ethanol and added to the HDS slurry under magnetic stirring. After reacting for 10
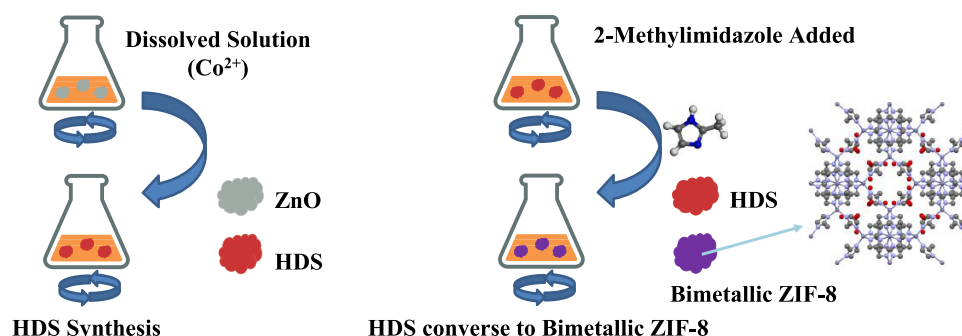
Figure 1. Schematic illustration of the HDS conversion method for bimetallic ZIF-8.

min, the product was separated by centrifugation at 6000 rpm for 3 min and washed three times with 50 mL of ethanol. All operations were conducted at room temperature. The collected purple powder was dried in a vacuum at 60 °C for 12 h, and the resulting product was designated as bimetallic ZIF-8.

2.2.3. Synthesis of One-pot ZIF-8/67. First, dissolve 0.1 g (0.386 mmol) of $Zn(NO_3)_2 \cdot 6H_2O$ and 0.1 g (0.339 mmol) of $Co(NO_3)_2 \cdot 6H_2O$ in 20 mL of deionized water, and use ultrasound treatment for 10 min to ensure complete dissolution. Next, dissolve 1 g (12.25 mmol) of 2-methylimidazole in 10 mL of ethanol and slowly add it to the metal ion solution. Magnetically stir at room temperature for 30 min to ensure the reaction proceeds fully. Centrifuge the reaction product at 6000 rpm, wash three times with ethanol, and dry the collected Onepot-ZIF-8/67 under vacuum at 60 °C for 12 h.

2.2.4. Synthesis of ZIF-8. Dissolve 0.1 g (0.386 mmol) of $Zn(NO_3)_2 \cdot 6H_2O$ in 10 mL of deionized water using ultrasound treatment for complete dissolution. Next, dissolve 0.5 g (6.1 mmol) of 2-methylimidazole in 10 mL of ethanol and slowly add it to the Zn ion solution. Magnetically stir for 10 min at room temperature, then centrifuge at 6000 rpm to separate the solid product, washing three times with ethanol. Dry the collected ZIF-8 powder under vacuum at 60 °C for 12 h.

2.2.5. Synthesis of ZIF-67. Dissolve 0.1 g (0.339 mmol) of $Co(NO_3)_2 \cdot 6H_2O$ in 10 mL of deionized water using ultrasound treatment to ensure complete dissolution. Next, dissolve 0.5 g (6.1 mmol) of 2-methylimidazole in 10 mL of ethanol and slowly add it to the Co ion solution. Magnetically stir for 10 min at room temperature, Centrifuge at 6000 rpm to separate the solid product, and wash three times with ethanol. Dry the collected ZIF-67 powder under vacuum at 60 °C for 12 h.

2.2.6. Control of Bimetallic ZIF-8 Particle Size. 0.05 g of CoZnHDS was dispersed in a mixture of deionized water and ethanol (v%/v% = 50:50) using ultrasound treatment for a specified duration. Then, 0.5 g (6.1 mmol) of 2-methyl-imidazole was dissolved in an appropriate amount of ethanol and added to the HDS slurry under magnetic stirring. After reacting for the specified time, the product was separated by centrifugation at 6000 rpm for 3 min and washed three times with 50 mL of ethanol. The particle size and dispersibility of the obtained product are provided in the Supporting Information Table.

2.2.7. Copper Ion Adsorption Experiment Procedure and Calculation Formulas. To evaluate the copper ion adsorption capacity, 30 mg of the sample was used as the adsorbent. A standard copper solution was prepared by dissolving copper

acetate in distilled water to achieve a concentration of 1000 mg/L. The adsorption experiment was conducted by adding the 30 mg of adsorbent to 50 mL of the copper solution and stirring the mixture at 60 °C. Samples were taken at varying time intervals, approximately every 30 s, to monitor the copper concentration using UV−vis spectroscopy at a wavelength of 750 nm.

2.3. Characterization. X-ray diffraction (XRD) was performed using a PANalytical X'Pert PRO X-ray diffrac-tometer (Cu Kα radiation source) at an operating voltage of 40 kV, with a scanning range of 5−50° and a scanning speed of 4°/min. Scanning electron microscopy (SEM) images were taken with a Hitachi SU-8010 SEM. Before imaging, the powder samples were dispersed in ethanol, dropped onto polished silicon wafers, and coated with platinum by sputtering. Energy-dispersive X-ray (EDX) analysis was performed using an Oxford energy-dispersive X-ray spectrom-eter (X-max80) equipped on the SU-8010 SEM. Transmission electron microscopy (TEM) images were taken with a Hitachi HT-7700. Before imaging, the powder samples were dispersed in ethanol and dropped onto a carbon support film. The Co:Zn ratio in HDS and ZIF powders was determined by inductively coupled plasma optical emission spectrometry (ICP-OES, Varian-730ES). 0.020 g of powder sample was dissolved in 1 mL of HNO_3 (65% to 68%, Sinopharm) and diluted to 100 mL (<20 ppm). Before ICP-OES analysis, the sample solution was filtered using a 0.2 μm filter. The BET surface area was calculated from N_2 adsorption measurements performed at 77 K using a Quantachrome Autosorb-IQ2-MP gas adsorption analyzer. Particle size and size distribution were measured using a Zetasizer 3000HSA (Marven) nanoparticle size analyzer. Fourier transform infrared spectroscopy (FTIR) was measured using a Thermo Nicolet 5700 spectrometer. The thermal stability of the samples was measured using a Mettler TGA/DSC3+ simultaneous thermal analyzer (TGA). Ultraviolet−visible diffuse reflectance spectroscopy (UV−vis) was measured using a PerkinElmer Lambda 750 spectrometer.

3. RESULTS AND DISCUSSION

Figure 1 illustrates the room temperature conversion route of the HDS method for synthesizing bimetallic ZIF-8. In this process, zinc oxide first reacts with cobalt nitrate to form HDS, followed by the addition of an organic ligand to convert it into ZIF-8 structure. Morphological analysis of the synthesized HDS was conducted using SEM, TEM, and AFM, revealing a typical layered structure with a thickness of approximately 3 nm. The morphology of bimetallic ZIF-8 synthesized from HDS precursors was analyzed by SEM, which showed uniform particle morphology (Figure 3e). SEM images revealed that
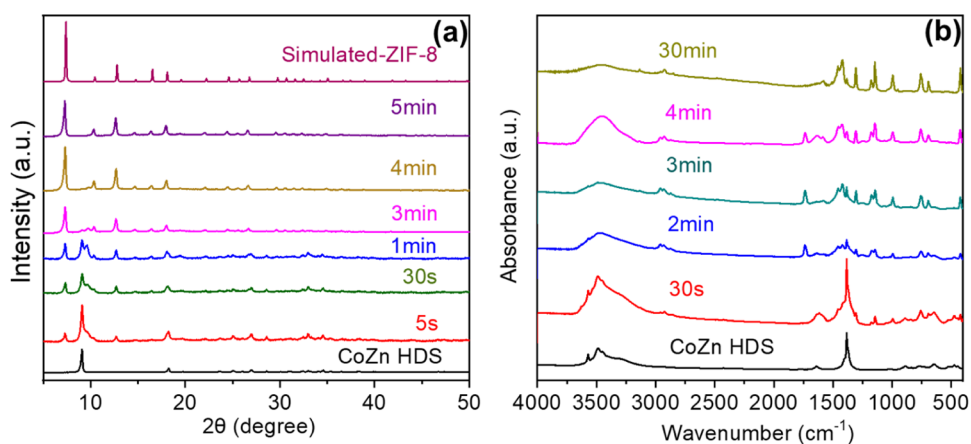
Figure 2. (a) XRD and (b)FTIR patterns of the intermediates collected during the conversion of CoZnHDS in 2-methylimidazole solution at different reaction time.
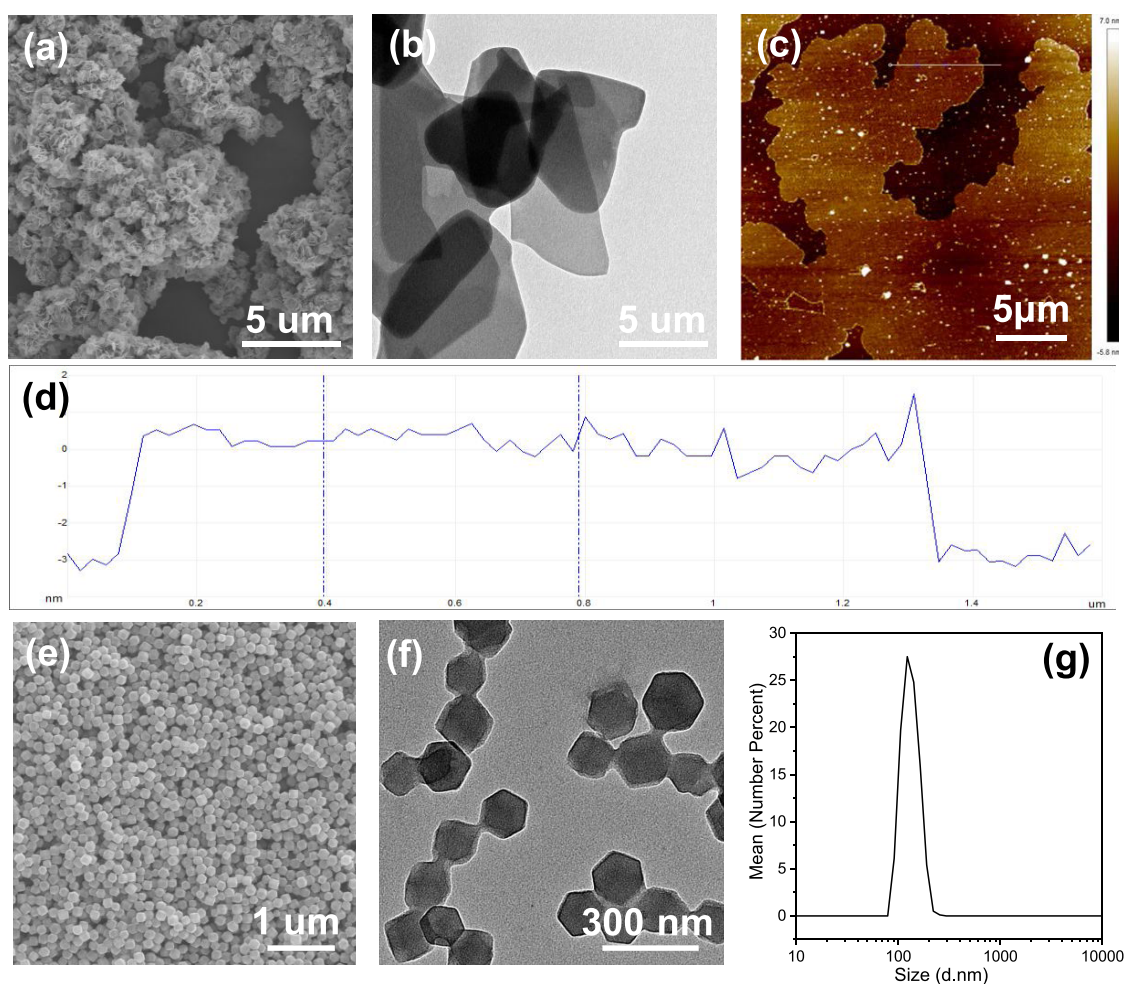
Figure 3. Morphological and Structural Characterization of ZIF-8 Synthesized from HDS Precursor. (a) SEM of HDS; (b) TEM of HDS; (c) AFM of HDS; (d) Thickness of HDS; (e) SEM of bimetallic ZIF-8; (f) TEM of bimetallic ZIF-8; (g) DLS of bimetallic ZIF-8.

bimetallic ZIF-8 particles exhibited a regular polyhedral structure with smooth surfaces. TEM images (Figure 3f) revealed the internal structure and crystalline morphology of the bimetallic ZIF-8 particles, showcasing clear crystal boundaries and uniform internal structures. Measurement of particles in SEM images indicated that the particle size of bimetallic ZIF-8 was 136.5 ± 12 nm, demonstrating good size

uniformity. To further verify the size distribution of bimetallic ZIF-8 particles, dynamic light scattering (DLS) tests were conducted. The DLS results showed an average particle size of 135 nm with a polydispersity index (PDI) of 0.024, indicating a very narrow size distribution. It was consistent with the SEM measurements, confirming that the synthesis method based on
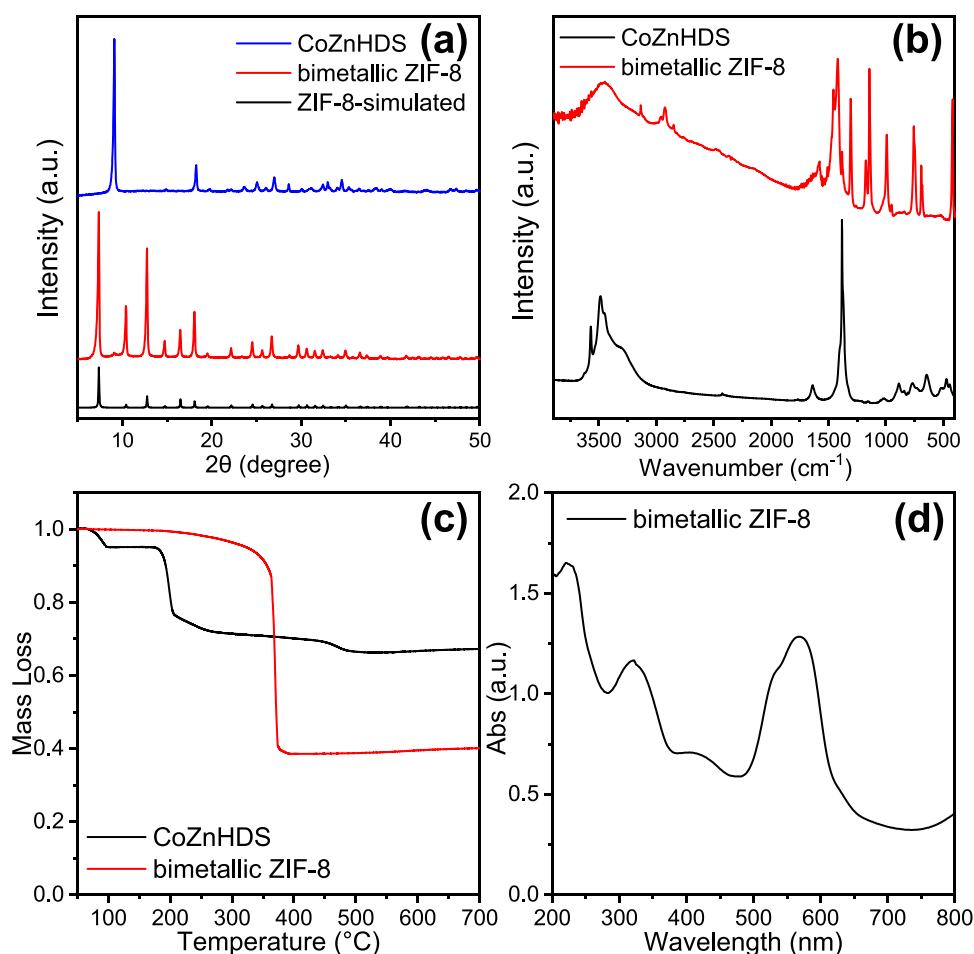
Figure 4. Structural and Performance Characterization of bimetallic ZIF-8 Synthesized from HDS Precursor. (a) XRD patterns of simulated ZIF-8, synthesized bimetallic ZIF-8, and HDS; (b) FTIR spectra of bimetallic ZIF-8 and HDS; (c) TGA curves of bimetallic ZIF-8 and HDS; (d) UV–vis spectrum of bimetallic ZIF-8.

HDS precursors effectively produces uniformly sized bimetallic ZIF-8 particles.

We investigated the transformation mechanism of CoZnHDS to bimetallic ZIF-8, as demonstrated by a series of semi-in situ XRD and FTIR analyses. Figure 2a shows the XRD patterns of samples at different reaction times, indicating a rapid transformation of CoZnHDS into bimetallic ZIF-8 within 5 min. During this process, the diffraction peak at 9.08°, associated with HDS(200), gradually disappeared, confirming the conversion to bimetallic ZIF-8. The transient appearance of a peak at 9.57°, followed by its disappearance, suggests the formation of an intermediate phase, likely a modified HDS structure with reduced interlayer spacing due to anion exchange. This intermediate phase supports the hypothesis that anion exchange is the initial step in the transformation of HDS into the MOF structure.

Further insights are provided in Figure 2b, which displays FTIR spectra at different reaction times. A peak at 1732.8 cm^{-1}, corresponding to an intermediate phase, appears briefly and then vanishes, mirroring changes seen in the XRD patterns. The increasing intensity of absorption peaks in the 1300−1400 cm^{-1} range indicates the penetration and reaction of 2-methylimidazole within the HDS interlayers. Moreover, the emergence of peaks in the 420−450 cm^{-1} range, indicative of Co/Zn−N bonds, confirms the coordination of 2-

methylimidazole with Zn^{2+} and Co^{2+} ions, leading to the formation of bimetallic ZIF-8.

Additionally, SEM imaging was used to examine the morphology of the intermediates during the reaction. SEM images (Figure S1, complemented by Figure 3) reveal the material's morphological evolution from the layered structure of HDS to finely dispersed mm-sized ZIF-8 particles. Notably, the SEM image of the sample reacted for 3 min shows intermediates where ZIF particles are emerging within the layered structure, interconnected by partially unconverted HDS, providing a visual confirmation of the transformation process.

The EDX mapping (Figure S3) and ICP-OES results confirm that the metal ratio in both CoZnHDS and bimetallic ZIF-8 is approximately consistent (Co/Zn ≈ 1:2). These characterization results indicate that the rapid room-temperature method of producing bimetallic ZIF-8 from HDS precursors has significant advantages, resulting in high-quality and uniformly sized bimetallic ZIF-8 particles.

Structural and performance characterization of bimetallic ZIF-8 synthesized from HDS precursor are illustrated in Figure 4. The XRD patterns (Figure 4a) of simulated ZIF-8, synthesized bimetallic ZIF-8, and CoZnHDS are shown. The XRD pattern of HDS exhibits a distinct peak at 9.05°, consistent with the characteristic peak of HDS reported in the literature.[46,47] The XRD pattern of synthesized bimetallic ZIF-

8 shows multiple characteristic peaks at 7.3, 10.4, 12.7, and 14.7°, which match well with those of simulated ZIF-8, indicating that the synthesized material is ZIF-8 structure with good crystallinity. This confirms the successful conversion of CoZnHDS precursor to ZIF-8 and that ZIF-8 possesses the expected crystalline structure.

The FTIR spectra (Figure 4b) of bimetallic ZIF-8 and CoZnHDS are also presented. The FTIR spectrum of HDS shows distinct peaks at 1381.94, 3482, and 3571.4 cm^{-1}. The sharp peaks at 3482 and 3571.4 cm^{-1} are attributed to $-$OH stretching vibrations, while the peak at 1381.94 cm^{-1} is likely associated with the characteristic vibrations of the hydroxide double salt in HDS. The FTIR spectrum of bimetallic ZIF-8 shows multiple characteristic peaks, reflecting its complex molecular structure. The main peaks are assigned as follows: 425 cm^{-1} is related to Zn$-$N or Co$-$N stretching vibrations; 689.7 and 755.8 cm^{-1} are possibly due to Zn$-$N or Co$-$N coordination vibration modes; 958.3 and 996.94 cm^{-1} are likely associated with imidazole ring deformation vibrations; 1142.8 and 1173.9 cm^{-1} are assigned to C$-$N stretching vibrations; 1306.1 and 1426.7 cm^{-1} are linked to C$-$H bending vibrations within the imidazole ring; 1584.2 cm^{-1} is related to C$=$C or C$=$N stretching vibrations; and the broad peak at 3450.8 cm^{-1} is due to hydrogen bonding and residual water molecules in the ZIF-8 structure. These FTIR peaks indicate that the synthesized bimetallic ZIF-8 possesses the expected chemical bonds and molecular structure.

Figure 4c shows the thermogravimetric analysis (TGA) curves of bimetallic ZIF-8 and HDS. The TGA curve of HDS shows two weight loss stages before 200 °C, corresponding to the removal of adsorbed water and structural water, with a decomposition temperature around 450 °C. In contrast, the TGA curve of bimetallic ZIF-8 shows a single weight loss plateau at 350 °C, corresponding to the decomposition of the ZIF-8 framework, indicating that the product is a uniform bimetallic ZIF-8 framework, rather than the mixture of ZIF-8 and ZIF-67. The UV$-$vis spectrum (Figure 4d) of bimetallic ZIF-8 displays multiple absorption peaks. The absorption peak at 224 nm typically corresponds to $\pi-\pi^*$ transitions, indicating the presence of a conjugated system in ZIF-8; the peak at 321 nm possibly corresponds to n-π^* transitions, reflecting the transition of nonbonding electrons in the ZIF-8 structure; the peak at 418 nm is likely related to metal-to-ligand charge transfer (MLCT) in ZIF-8;[48] and the absorption peaks at 530 and 569 nm are possibly related to d-d transitions of metal ions in bimetallic ZIF-8, particularly the electronic transitions of Co and Zn elements doped in bimetallic ZIF-8. These absorption peaks indicate that the synthesized ZIF-8 has a complex electronic structure and promising optical properties, making it potentially valuable in photocatalysis and optical materials applications.

Shown in Figure 5 is the nitrogen adsorption isotherm of bimetallic ZIF-8 synthesized from CoZnHDS. The BET surface area calculated from this adsorption isotherm of ZIF-8 is 1463.78 cm^2/g, which is consistent with the BET surface area of bimetallic ZIF-8 reported in the literature.[49] Using the aforementioned characterization techniques, we confirmed that the bimetallic ZIF-8 synthesized from HDS precursors has uniform particle size, good crystallinity, and stable structure. Additionally, it exhibits self-assembly properties and excellent optical characteristics.

The different self-assembly methods of bimetallic ZIF-8 are displayed in Figure 6. Illustrated in Figure 6a is the three-
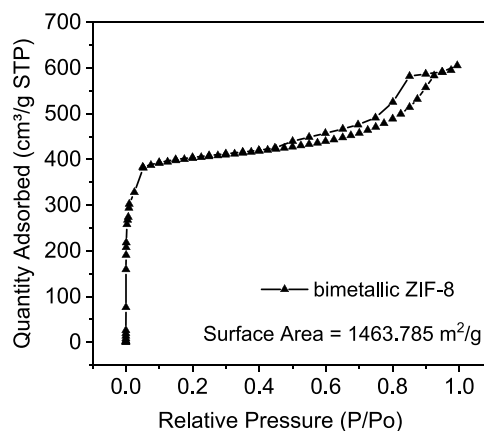

Figure 5. N$_2$ physisorption isotherm at 77 K for the bimetallic ZIF-8 obtained from HDS.

dimensional self-assembly achiedved by depositing the sample, at a concentration of 20 mg/mL, onto a silicon wafer and allowing the solvent to evaporate slowly at room temperature. The bimetallic ZIF-8 particles exhibit a rhombic dodecahedron structure and form an ordered three-dimensional arrangement through facet-to-facet attraction. Figure 6b shows the planar self-assembly formed by adding 20 μL of oleic acid to 1 mL of the same sample as in (a), then depositing it onto a silicon wafer and allowing the solvent to evaporate slowly at room temperature. This method results in the ZIF-8 particles forming an ordered two-dimensional planar arrangement on the surface. Figure 6c presents a schematic diagram of the self-assembly potential, visually illustrating the structures formed by the different self-assembly methods of the bimetallic ZIF-8 particles. Figure S2 shows the sample prepared by dispersing in DMF, which also exhibits a tendency for planar self-assembly on the surface. These results indicate that by adjusting solvent evaporation conditions and additives, the self-assembly morphology of bimetallic ZIF-8 can be controlled, thereby influencing its performance in different applications.

The HDS conversion method can produce uniformly sized nanoparticles for the following reasons: Crystal formation involves nucleation and crystal growth.[50] Using HDS as an intermediate provides numerous active sites for the coordination of organic ligands,[43,51] effectively reducing the nucleation time to almost zero. Therefore, the growth time of all crystals can be considered the same within a certain range, resulting in uniformly sized crystals.

We also investigated the effect of synthesis conditions on the particle size distribution of bimetallic ZIF-8 by altering the synthesis parameters. A series of synthesis conditions were designed based on a reaction time of 30 min and a 2-methylimidazole concentration of 0.41 mol/L. As shown in Table S1, with the increase in ultrasonic time, the PDI of the product initially decreased from 0.103 to 0.024, but then sharply increased to 0.260 when the ultrasonic time exceeded 40 min. This trend is primarily due to the influence of ultrasonic time on the thickness and dispersibility of the HDS layers. During the initial extension of ultrasonic time, thin HDS layers may exfoliate from the bulk structure, forming uniformly thick and well-dispersed precursors. However, with prolonged ultrasonic time, excessive ultrasonic energy may lead to the destruction of the nanosheet structure or the aggregation of nanoparticles. Through extensive repeated experiments, it was found that an ultrasonic time of 40 min resulted in the lowest
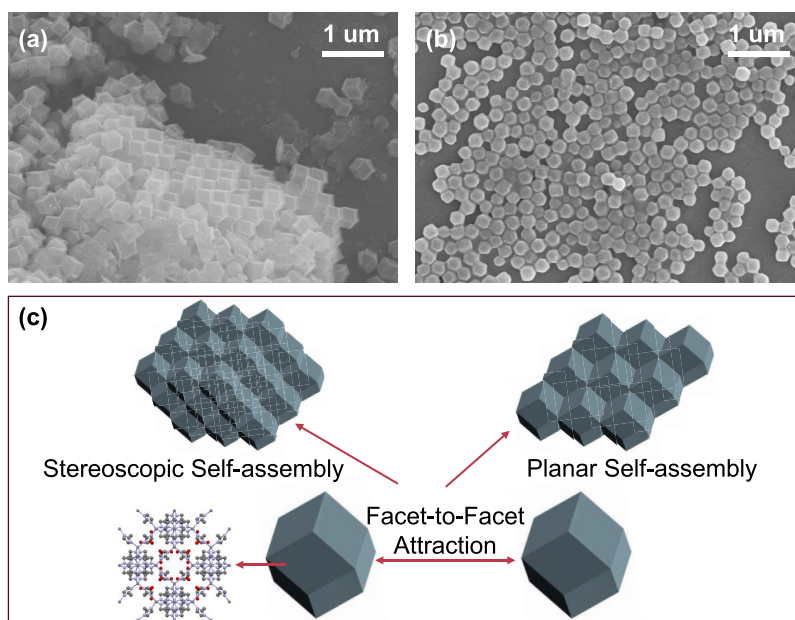
Figure 6. Three-dimensional and planar self-assembly potential of bimetallic ZIF-8: (a) Three-dimensional self-assembly after depositing the sample at a concentration of 20 mg/mL onto a silicon wafer and allowing the solvent to evaporate slowly at room temperature; (b) Planar self-assembly after adding 20 μL of oleic acid to 1 mL of the same sample as in (a), then depositing it onto a silicon wafer and allowing the solvent to evaporate slowly at room temperature; (c) Schematic diagram of the self-assembly.
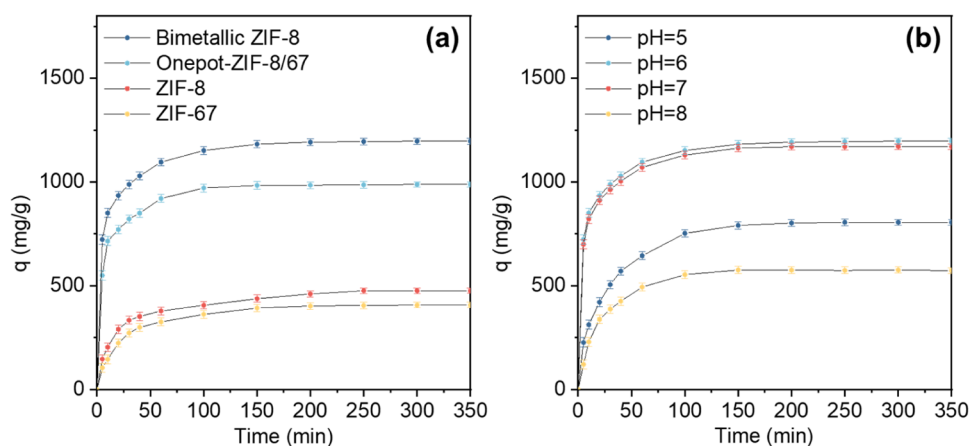
Figure 7. (a) Adsorption curves of bimetallic ZIF-8, Onepot-ZIF-8/67, ZIF-8, and ZIF-67 for copper ions at pH 6; (b) Adsorption curves of bimetallic ZIF-8 for copper ions under various pH conditions.

PDI of 0.024 and a particle size of 135.0 nm. Therefore, an ultrasonic time of 40 min was adopted for subsequent studies.

In addition to ultrasonic time, different concentrations of 2-methylimidazole were also used: 0.20 mol/L, 0.41 mol/L, and 0.81 mol/L, with the ultrasonic time for HDS prepared by the hydrolysis method set to 40 min and a reaction time of 30 min. As shown in Table S2, the PDI of the product initially improves and then worsens with increasing reactant concentration. The main reason is that at higher reactant concentrations, the formation rate of bimetallic ZIF-8 particles is too rapid, while at lower concentrations, the conversion of CoZnHDS to bimetallic ZIF-8 is too slow or incomplete. After numerous repetitive experiments (each set of experiments repeated more than three times), it was found that at a 2-methylimidazole concentration of 0.41 mol/L, the product had the lowest PDI of 0.024 and a particle size of 135.0 nm.

We further investigated the effect of different reaction times (ranging from 5 to 45 min) on the particle size distribution of bimetallic ZIF-8, with the ultrasonic time for HDS prepared by the hydrolysis method set to 40 min and a 2-methylimidazole concentration of 0.41 mol/L. As shown in Table S3, with increasing reaction time, the PDI of the product initially decreases from 0.632 to 0.024, but then increases to 0.083 when the reaction time exceeds 30 min. At a reaction time of 30 min, the product has the lowest PDI of 0.024 and a particle size of 135.0 nm. At shorter reaction times, CoZnHDS has not fully or has just converted to bimetallic ZIF-8 particles, resulting in a relatively wide PDI. When the reaction time is too long, Ostwald ripening or aggregation due to nanoparticle collisions may cause the PDI to widen.[52]

Using the aforementioned characterization techniques, we confirmed that the bimetallic ZIF-8 synthesized from HDS precursors exhibits uniform particle size, good crystallinity, and

a stable structure. Additionally, its self-assembly performance and excellent optical properties were demonstrated. These results indicate that the rapid room-temperature synthesis method of bimetallic ZIF-8 from HDS precursors has significant advantages, enabling the production of high-quality and uniformly sized bimetallic ZIF-8 particles. This provides a solid foundation for their application in catalysis, gas separation, and energy storage. With further optimization and control, this method is expected to play an important role in the broader synthesis of MOF materials.

The adsorption performance of different ZIF structures for copper ions at pH 6 is shown in Figure 7a. ZIF-67 exhibited the lowest adsorption capacity, while ZIF-8 showed a moderate improvement. The Onepot-ZIF-8/67, synthesized via a one-pot method, further enhanced adsorption capacity, reflecting the synergistic effect of incorporating both Zn and Co. Notably, bimetallic ZIF-8 achieved the highest adsorption capacity of 1196.82 mg/g, indicating that the presence of multiple active sites significantly improves copper ion removal efficiency.

We also evaluated the adsorption performance of bimetallic ZIF-8 across different pH levels (Figure 7b). The highest capacity was observed at pH 6, with slightly lower but comparable results at pH 7. Adsorption efficiency decreased at pH 5 and was lowest at pH 8, likely due to copper hydroxide precipitation in alkaline conditions, which reduces the availability of free copper ions for adsorption. These results suggest that slightly acidic to neutral pH conditions are optimal for copper ion uptake by bimetallic ZIF-8. Figure S4 presents the SEM and EDS analysis of ZIF-8 after Cu^{2+} adsorption at pH 7. The SEM images reveal that the samples have undergone some degree of aggregation after Cu^{2+} adsorption. However, the XRD results indicate no significant changes in the crystallographic structure of ZIF-8 after the adsorption process, suggesting that the integrity of the material is largely maintained despite the observed aggregation.

In order to provide a comprehensive evaluation of our bimetallic ZIF-8's performance in Cu^{2+} adsorption, we have compared it with other widely reported composite materials, such as Alginate-chitosan/hydroxyapatite and Sodium alginate/sodium humate @ Polyacrylamide.[18−20] As shown in Table 2, our material demonstrates significantly higher

Table 2. Comparison of Cu^{2+} Adsorption Performance between Bimetallic ZIF-8 and Other Composite Adsorbents

sample name	Cu^{2+} adsorption capacity (mg/g)	refs
Co@ZIF-8	1191.67	18
alginate-chitosan/hydroxyapatite	208.34	19
sodium alginate/sodium humate @ polyacrylamide	134.65	20
Bimetallic ZIF-8	1196.82	this work

adsorption capacity. However, these composite materials exhibit superior recyclability due to their inherent biodegradable and structural properties. Compared to previously reported ZIF-8-based materials, our bimetallic ZIF-8 shows comparable adsorption efficiency, emphasizing the benefits of the HDS transformation strategy employed in our study.

4. CONCLUSIONS

Using various characterization techniques, we confirmed that ZIF-8 synthesized from HDS precursors possesses uniform particle size, good crystallinity, and a stable structure. Further studies revealed that ultrasonic time, 2-methylimidazole concentration, and reaction time are key factors affecting the size and dispersibility of ZIF-8. Under optimized conditions, the synthesized ZIF-8 particles have a size of 135.0 nm and a PDI of 0.024. Additionally, the copper ion adsorption experiments highlighted the material's strong performance at slightly acidic to neutral pH levels, further emphasizing its potential in environmental applications. In summary, the rapid room-temperature synthesis method for ZIF-8 using HDS precursors has significant advantages, enabling the production of high-quality and uniformly sized ZIF-8 particles. This provides a solid foundation for their application in catalysis, gas separation, and energy storage and heavy metal remediation. With further optimization and control, this method is expected to play an important role in the broader synthesis of MOF materials.

■ ASSOCIATED CONTENT

Ⓢ Supporting Information

The Supporting Information is available free of charge at https://pubs.acs.org/doi/10.1021/acsomega.4c06512.

> SEM images of CoZnHDS reacted with 2-methylimidazole for 3 min (Figure S1). SEM of ZIF-8 dispersed in DMF and dried on a silicon wafer (Figure S2). SEM and EDS data for CoZnHDS and ZIF-8 (Figure S3). ZIF-8 particle size distribution based on different ultrasonication times (Table S1). ZIF-8 particle size distribution using varying 2-methylimidazole concentrations (Table S2). ZIF-8 particle size and PDI data obtained with different reaction times (Table S3). SEM, EDS and XRD of ZIF-8 after Cu2+ adsorption at pH 7 (Figure S4) (PDF)

■ AUTHOR INFORMATION

Corresponding Author

Sheng Chu − *School of Materials Science and Engineering, Sun Yat-Sen University, Guangzhou 510006, China;* ⓘ orcid.org/0000-0001-7934-396X; Email: chusheng@mail.sysu.edu.cn

Authors

Yixin Chen − *School of Materials Science and Engineering, Sun Yat-Sen University, Guangzhou 510006, China;* ⓘ orcid.org/0000-0001-9678-058X

Zexi Chen − *School of Materials Science and Engineering, Sun Yat-Sen University, Guangzhou 510006, China*

Complete contact information is available at:
https://pubs.acs.org/10.1021/acsomega.4c06512

Notes

The authors declare no competing financial interest.

■ ACKNOWLEDGMENTS

■ REFERENCES

(1) Jiao, L.; Wang, Y.; Jiang, H.-L.; Xu, Q. Metal-Organic Frameworks as Platforms for Catalytic Applications. *Adv. Mater.* **2018**, *30*, No. 1703663.

(2) Song, Q.; Nataraj, S. K.; Roussenova, M. V.; Tan, J. C.; Hughes, D. J.; Li, W.; Bourgoin, P.; Alam, M. A.; Cheetham, A. K.; Al-Muhtaseb, S. A.; Sivaniah, E. Zeolitic imidazolate framework (ZIF-8) based polymer nanocomposite membranes for gas separation. *Energy Environ. Sci.* **2012**, *5*, 8359−8369.

(3) Sankar, S. S.; Karthick, K.; Sangeetha, K.; Karmakar, A.; Kundu, S. Transition-Metal-Based Zeolite Imidazolate Framework Nanofibers via an Electrospinning Approach: A Review. *ACS Omega* **2020**, *5*, 57−67.

(4) Li, K.; Miwornunyuie, N.; Chen, L.; Jingyu, H.; Amaniampong, P. S.; Ato Koomson, D.; Ewusi-Mensah, D.; Xue, W.; Li, G.; Lu, H. Sustainable Application of ZIF-8 for Heavy-Metal Removal in Aqueous Solutions. *Sustainability* **2021**, *13*, 984.

(5) Yang, W.; Kong, Y.; Yin, H.; Cao, M. Study on the adsorption performance of ZIF-8 on heavy metal ions in water and the recycling of waste ZIF-8 in cement. *J. Solid State Chem.* **2023**, *326*, No. 124217.

(6) Zhao, Y.; Pan, Y.; Liu, W.; Zhang, L. Removal of Heavy Metal Ions from Aqueous Solutions by Adsorption onto ZIF-8 Nanocrystals. *Chem. Lett.* **2015**, *44*, 758−760.

(7) Mo, Z.; Tai, D.; Zhang, H.; Shahab, A. A comprehensive review on the adsorption of heavy metals by zeolite imidazole framework (ZIF-8) based nanocomposite in water. *Chem. Eng. J.* **2022**, *443*, No. 136320.

(8) Chen, H.; Wang, J. MOF-derived Co3O4-C@FeOOH as an efficient catalyst for catalytic ozonation of norfloxacin. *J. Hazard. Mater.* **2021**, *403*, No. 123697.

(9) Matsuoka, A.; Matsumura, H.; Odaka, M.; Ogawa, N.; Tanno, T. The Transitional Transmittance Response of ZIF-8 Gas Adsorption Observed Using Terahertz Waves. *e-J. Surf. Sci. Nanotechnol.* **2018**, *16*, 142−144.

(10) Samadi-Maybodi, A.; Ghasemi, S.; Ghaffari-Rad, H. A novel sensor based on Ag-loaded zeolitic imidazolate framework-8 nano-crystals for efficient electrocatalytic oxidation and trace level detection of hydrazine. *Sens. Actuators, B* **2015**, *220*, 627−633.

(11) Awadallah-F, A.; Hillman, F.; Al-Muhtaseb, S. A.; Jeong, H.-K. On the nanogate-opening pressures of copper-doped zeolitic imidazolate framework ZIF-8 for the adsorption of propane, propylene, isobutane, and n-butane. *J. Mater. Sci.* **2019**, *54*, 5513−5527.

(12) Xiang, Y.; Yu, D.; Qin, C.; Deng, J.; Wang, X.; Ge, B.; Huang, F. Bimetallic zeolitic imidazolate frameworks Co/ZIF-8 crystals as carbonic anhydrase-mimicking nanozyme. *Colloids Surf., A* **2024**, *685*, No. 133227.

(13) Villajos, J. A.; Orcajo, G.; Martos, C.; Botas, J.Á.; Villacañas, J.; Calleja, G. Co/Ni mixed-metal sited MOF-74 material as hydrogen adsorbent. *Int. J. Hydrogen Energy* **2015**, *40*, 5346−5352.

(14) Schneemann, A.; Rudolf, R.; Baxter, S. J.; Vervoorts, P.; Hante, I.; Khaletskaya, K.; Henke, S.; Kieslich, G.; Fischer, R. A. Flexibility control in alkyl ether-functionalized pillared-layered MOFs by a Cu/Zn mixed metal approach. *Dalton Trans.* **2019**, *48*, 6564−6570.

(15) Gao, J.; Qian, X.; Lin, R.-B.; Krishna, R.; Wu, H.; Zhou, W.; Chen, B. Mixed Metal−Organic Framework with Multiple Binding Sites for Efficient C2H2/CO2 Separation. *Angew. Chem., Int. Ed.* **2020**, *59*, 4396−4400.

(16) Masoomi, M. Y.; Morsali, A.; Dhakshinamoorthy, A.; Garcia, H. Mixed-Metal MOFs: Unique Opportunities in Metal−Organic Framework (MOF) Functionality and Design. *Angew. Chem., Int. Ed.* **2019**, *58*, 15188−15205.

(17) Abednatanzi, S.; Gohari Derakhshandeh, P.; Depauw, H.; Coudert, F.-X.; Vrielinck, H.; Van Der Voort, P.; Leus, K. Mixed-metal metal−organic frameworks. *Chem. Soc. Rev.* **2019**, *48*, 2535−2565.

(18) Shen, B.; Wang, B.; Zhu, L.; Jiang, L. Properties of Cobalt- and Nickel-Doped Zif-8 Framework Materials and Their Application in Heavy-Metal Removal from Wastewater. *Nanomaterials* **2020**, *10*, 1636.

(19) Jioui, I.; Abrouki, Y.; Aboul Hrouz, S.; Sair, S.; Dânoun, K.; Zahouily, M. Efficient removal of Cu2+ and methylene blue pollutants from an aqueous solution by applying a new hybrid adsorbent based on alginate-chitosan and HAP derived from Moroccan rock phosphate. *Environ. Sci. Pollut. Res.* **2023**, *30*, 107790−107810.

(20) Wang, H.; Huang, M.; Li, L.; Wang, B.; Jiang, C.; Hu, X.; Xie, Y.; Chen, R.; Guo, W.; Xiao, H.; Wang, M.; Zhou, D. Highly efficient copper ions removal by sodium alginate/sodium humate@Poly-acrylamide: adsorption behavior and removal mechanism. *Water, Air, Soil Pollut.* **2024**, *235*, No. 250.

(21) Zadehahmadi, F.; Eden, N. T.; Mahdavi, H.; Konstas, K.; Mardel, J. I.; Shaibani, M.; Banerjee, P. C.; Hill, M. R. Removal of metals from water using MOF-based composite adsorbents. *Environ. Sci.: Water Res. Technol.* **2023**, *9*, 1305−1330.

(22) Haso, H. W.; Dubale, A. A.; Chimdesa, M. A.; Atlabachew, M. High Performance Copper Based Metal Organic Framework for Removal of Heavy Metals From Wastewater. *Front. Mater.* **2022**, *9*, No. 840806, DOI: 10.3389/fmats.2022.840806.

(23) Ban, Y.; Li, Y.; Peng, Y.; Jin, H.; Jiao, W.; Liu, X.; Yang, W. Metal-Substituted Zeolitic Imidazolate Framework ZIF-108: Gas-Sorption and Membrane-Separation Properties. *Chem. - Eur. J.* **2014**, *20*, 11402−11409.

(24) Wang, C.; Yang, F.; Sheng, L.; Yu, J.; Yao, K.; Zhang, L.; Pan, Y. Zinc-substituted ZIF-67 nanocrystals and polycrystalline membranes for propylene/propane separation. *Chem. Commun.* **2016**, *52*, 12578−12581.

(25) Sun, Y.; Huang, H.; Guo, X.; Qiao, Z.; Zhong, C. Controlling Metal Ion Counter Diffusion in Confined Spaces for In Situ Growth of Mixed Metal MOF Membranes for Gas Separation. *ChemNanoMat* **2019**, *5*, 1244−1250.

(26) Song, G.; Kenney, M.; Chen, Y.-S.; Zheng, X.; Deng, Y.; Chen, Z.; Wang, S. X.; Gambhir, S. S.; Dai, H.; Rao, J. Carbon-coated FeCo nanoparticles as sensitive magnetic-particle-imaging tracers with photothermal and magnetothermal properties. *Nat. Biomed. Eng.* **2020**, *4*, 325−334.

(27) Zhong, X.-f.; Sun, X. Nanomedicines based on nanoscale metal-organic frameworks for cancer immunotherapy. *Acta Pharmacol. Sin.* **2020**, *41*, 928−935.

(28) Zeng, C.; Chen, Y.; Kirschbaum, K.; Lambright, K. J.; Jin, R. Emergence of hierarchical structural complexities in nanoparticles and their assembly. *Science* **2016**, *354*, 1580−1584.

(29) Yanai, N.; Granick, S. Directional Self-Assembly of a Colloidal Metal−Organic Framework. *Angew. Chem., Int. Ed.* **2012**, *51*, 5638−5641.

(30) Kim, D.; Park, J.; Park, J.; Jang, J.; Han, M.; Lim, S.-H.; Ryu, D. Y.; You, J.; Zhu, W.; Yamauchi, Y.; Kim, J. Surfactant-Free, Size-Controllable, and Scalable Green Synthesis of ZIF-8 Particles with Narrow Size Distribution by Tuning Key Reaction Parameters in Water Solvent. *Small Methods* **2024**, *8*, No. 2400236.

(31) Avci, C.; Imaz, I.; Carné-Sánchez, A.; Pariente, J. A.; Tasios, N.; Pérez-Carvajal, J.; Alonso, M. I.; Blanco, A.; Dijkstra, M.; López, C.; Maspoch, D. Self-assembly of polyhedral metal−organic framework particles into three-dimensional ordered superstructures. *Nat. Chem.* **2018**, *10*, 78−84.

(32) Loloei, M.; Kaliaguine, S.; Rodrigue, D. CO2-Selective mixed matrix membranes of bimetallic Zn/Co-ZIF *vs.* ZIF-8 and ZIF-67. *Sep. Purif. Technol.* **2022**, *296*, No. 121391.

(33) Joshi, B.; Samuel, E.; Kim, Y.; Periyasami, G.; Rahaman, M.; Yoon, S. S. Bimetallic zeolitic imidazolate framework-derived substrate-free anode with superior cyclability for high-capacity lithium-ion batteries. *J. Mater. Sci. Technol.* **2021**, *67*, 116−126.

(34) Gadipelli, S.; Li, Z.; Zhao, T.; Yang, Y.; Yildirim, T.; Guo, Z. Graphitic nanostructures in a porous carbon framework significantly enhance electrocatalytic oxygen evolution. *J. Mater. Chem. A* **2017**, *5*, 24686−24694.

(35) Trujillano, R.; Nieto, D.; Rives, V. Microwave-assisted synthesis of Ni, Zn layered double hydroxysalts. *Microporous Mesoporous Mater.* **2017**, *253*, 129−136.

(36) Chen, C.; Feng, X.; Zhu, Q.; Dong, R.; Yang, R.; Cheng, Y.; He, C. Microwave-Assisted Rapid Synthesis of Well-Shaped MOF-74 (Ni) for CO_2 Efficient Capture. *Inorg. Chem.* **2019**, *58*, 2717−2728.

(37) Wahiduzzaman, K.; Allmond, J.; Stone, S.; Harp, K.; Mujibur. Synthesis and Electrospraying of Nanoscale MOF (Metal Organic Framework) for High-Performance CO2 Adsorption Membrane. *Nanoscale Res. Lett.* **2017**, *12*, No. 6.

(38) Meek, S. T.; Greathouse, J. A.; Allendorf, M. D. Metal-Organic Frameworks: A Rapidly Growing Class of Versatile Nanoporous Materials. *Adv. Mater.* **2011**, *23*, 249−267.

(39) Zhang, R.; Tao, C.-A.; Chen, R.; Wu, L.; Zou, X.; Wang, J. Ultrafast Synthesis of Ni-MOF in One Minute by Ball Milling. *Nanomaterials* **2018**, *8*, 1067.

(40) Li, Z.; Cui, J.; Liu, Y.; Li, J.; Liu, K.; Shao, M. Electrosynthesis of Well-Defined Metal−Organic Framework Films and the Carbon Nanotube Network Derived from Them toward Electrocatalytic Applications. *ACS Appl. Mater. Interfaces* **2018**, *10*, 34494−34501.

(41) Polyzoidis, A.; Altenburg, T.; Schwarzer, M.; Loebbecke, S.; Kaskel, S. Continuous microreactor synthesis of ZIF-8 with high space−time-yield and tunable particle size. *Chem. Eng. J.* **2016**, *283*, 971−977.

(42) Meyn, M.; Beneke, K.; Lagaly, G. Anion-exchange reactions of hydroxy double salts. *Inorg. Chem.* **1993**, *32*, 1209−1215.

(43) Zhao, J.; Nunn, W. T.; Lemaire, P. C.; Lin, Y.; Dickey, M. D.; Oldham, C. J.; Walls, H. J.; Peterson, G. W.; Losego, M. D.; Parsons, G. N. Facile Conversion of Hydroxy Double Salts to Metal−Organic Frameworks Using Metal Oxide Particles and Atomic Layer Deposition Thin-Film Templates. *J. Am. Chem. Soc.* **2015**, *137*, 13756−13759.

(44) Duan, C.; Li, F.; Li, L.; Zhang, H.; Wang, X.; Xiao, J.; Xi, H. Hierarchically structured metal−organic frameworks assembled by hydroxy double salt−template synergy with high space−time yields. *CrystEngComm* **2018**, *20*, 1057−1064.

(45) Guo, Y.; Mao, Y.; Hu, P.; Ying, Y.; Peng, X. Self-confined synthesis of HKUST-1 membranes from CuO nanosheets at room temperature. *ChemistrySelect* **2016**, *1*, 108−113.

(46) Bull, R. M. R.; Markland, C.; Williams, G. R.; O'Hare, D. Hydroxy double salts as versatile storage and delivery matrices. *J. Mater. Chem.* **2011**, *21*, 1822−1828.

(47) Kandare, E.; Hossenlopp, J. M. Hydroxy Double Salt Anion Exchange Kinetics: Effects of Precursor Structure and Anion Size[†]. *J. Phys. Chem. B* **2005**, *109*, 8469−8475.

(48) Pattengale, B.; SantaLucia, D. J.; Yang, S.; Hu, W.; Liu, C.; Zhang, X.; Berry, J. F.; Huang, J. Direct Observation of Node-to-Node Communication in Zeolitic Imidazolate Frameworks. *J. Am. Chem. Soc.* **2018**, *140*, 11573−11576.

(49) Dai, Y.; Johnson, J. R.; Karvan, O.; Sholl, D. S.; Koros, W. J. Ultem/ZIF-8 mixed matrix hollow fiber membranes for CO_2/N_2 separations. *J. Membr. Sci.* **2012**, *401−402*, 76−82.

(50) Thanh, N. T. K.; Maclean, N.; Mahiddine, S. Mechanisms of Nucleation and Growth of Nanoparticles in Solution. *Chem. Rev.* **2014**, *114*, 7610−7630.

(51) Chen, Y.; Wu, H.; Xiao, Q.; Lv, D.; Li, F.; Li, Z.; Xia, Q. Rapid room temperature conversion of hydroxy double salt to MOF-505 for CO2 capture. *CrystEngComm* **2019**, *21*, 165.

(52) Shrestha, S.; Wang, B.; Dutta, P. Nanoparticle processing: Understanding and controlling aggregation. *Adv. Colloid Interface Sci.* **2020**, *279*, No. 102162.